Amorphization of metallic systems induced by low-temperature ion-beam mixing

J. Jagielski
Institute for Electronic Materials Technology, Wolczynska 133, 01-919 Warsaw, Poland

L. Thomé and T. Benkoulal
Centre de Spectrométrie Nucléaire et de Spectrométrie de Masse, Institut National de Physique Nucléaire et de Physique des Particules, Centre National de la Recherche Scientifique, Bâtiment 108, 91405 Orsay Campus, France
(Received 12 July 1993; revised manuscript received 25 March 1994)

Ion-beam mixing and amorphization were simultaneously studied via *in situ* Rutherford backscattering and channeling experiments on a Zr/Ni sample irradiated at low temperature with various medium-energy noble-gas ions. The number of mixed atoms and the spatial extension of the mixed layer were found to increase linearly with the nuclear energy density deposited by the irradiating ions. The existence of a threshold at 20 eV/Å provides an indication that a different mixing mechanism takes place in the case of very light ion irradiation. A good agreement is obtained between the experimental data and the predictions of a model based on a binary collision description. The channeling experiments devoted to the study of the amorphization process show that the concentration of foreign atoms introduced by mixing controls the amorphization kinetics. A possible mechanism for the amorphization process is presented. This mechanism is compared to that occurring in direct ion-implantation experiments.

I. INTRODUCTION

Ion bombardment of metallic compounds is known to induce atomic rearrangements which are responsible for the formation of new phases generally out of thermodynamical equilibrium. A typical example of ion-beam-induced phase transformation, driven by the radiation damage arising from elastic collisions between the incident ions and the target atoms, is the crystalline-to-amorphous transition.[1] Amorphization mechanisms by ion bombardment have been widely studied in the last years, and several models have been developed[2–7] to account for the large number of experimental results recorded on metal-metalloid and metal-metal systems.[8] Most of these models predict that amorphization results from the presence of both lattice disorder and foreign atoms acting as disorder stabilizers. The temperature T at which ion bombardment is performed was also demonstrated to be an important parameter for the study of the crystalline-to-amorphous transition since it governs the mobility of impurity atoms and defects.

Three types of experiments leading to the formation of an amorphous phase with an ion beam can be distinguished: ion irradiation, ion implantation, and ion-beam mixing. An attempt to reproduce the results obtained in the former two cases (irradiation and implantation) has been recently successfully performed.[9] This work has demonstrated that amorphization of metallic systems by ion bombardment results from the formation (and coalescence) of small clusters with a size and a composition depending on the bombardment conditions (ion mass, temperature, etc.). Moreover, it was established that the fraction of amorphous volume α at a given depth in the bombarded crystal is given by the product of two functions f and g, the first depending on the damage production d and the second on the concentration c of implanted foreign atoms:

$$\alpha = f(d,T)g(c,T) \ . \tag{1}$$

Thus radiation damage (function f) governs the formation of the amorphous clusters in irradiation experiments, while implanted ions (function g) control the amorphization kinetics in implantation experiments. The purpose of the present paper is to extend this study by the investigation of the amorphization processes occurring in the case of ion-beam mixing (outlines about this technique are given in Refs. 10–13).

The work presented here consists in irradiating a Zr/Ni bilayer at low temperature (in order to avoid thermally assisted effects) with several rare-gas ions of medium energy (which provide a wide range of nuclear energy loss) and in studying simultaneously by means of *in situ* Rutherford backscattering (RBS) and channeling experiments the mixing and amorphization of the target. The choice of Ni-Zr was dictated by the fact that (i) this system is known to be easily amorphized by ion bombardment,[14–16] (ii) good Ni single crystals are available for the channeling experiments, and (iii) the Zr peak and the Ni substrate are well separated in RBS experiments.

The study of the amorphization mechanisms by ion-beam mixing requires a detailed investigation of the mixing process itself. Such an investigation is presented in Sec. IV, where the results obtained are compared to the prediction of existing models. In Sec. V, the attention is focused on the kinetics of formation of the amorphous layer by ion-beam mixing and a comparison with the processes occurring in direct ion-implantation experiments.

A brief account of the first results has been given in Ref. 17.

II. CALCULATION OF COLLISION PARAMETERS

A natural scaling factor for the processes occurring during ion bombardment is the nuclear energy deposition density, usually denoted as ε. This parameter represents the energy deposited by the incoming ions in elastic collisions with the atom nuclei and thus accounts for the part of the ion energy lost for the displacement of target atoms. This quantity is frequently used to reduce mixing data or to scale the creation of radiation damage in order to compare the effects obtained in various ion-target couples.

The typical depth dependence of ε for a Zr/Ni bilayer irradiated with 450-keV Xe ions is presented in Fig. 1(a). It is worth noting that the choice of the accurate value of ε in the case of mixing experiments is not straightforward because of the large variation (a factor of ~2) taking place at the Zr/Ni interface. A value averaged between those selectively obtained in the Zr and Ni parts of the sample close to the interface is usually used in the literature. Nevertheless, it is quite clear that such a choice can lead to difficulties for comparing the results recorded with various irradiating ions, as is the case for the experiments reported here.

The values of ε used in this paper were determined by performing a TRIM simulation[18] in a trilayered $Zr/Zr_{0.5}Ni_{0.5}/Ni$ sample [see Fig. 1(b)]. The intermediate $Zr_{0.5}Ni_{0.5}$ layer was centered at the interface between the Zr layer and the Ni substrate, and a thickness of 200 Å was taken.[19] The choice of this procedure of calculation was imposed by the fact that, with the exception of the very early stages of the ion-mixing process where a sharp interface exists, displaced atoms originate mainly from an already mixed layer. The values of ε obtained in the intermediate layer for the various irradiations performed are listed in Table I.

Another parameter is essential in order to compare the experimental mixing results to the model predictions: the mean projected range of the displaced atoms R_d. The calculation was also done by running the TRIM code in a $Zr/Zr_{0.5}Ni_{0.5}/Ni$ sample identical to that used for the determination of ε. The simulation provides the mean energy of the recoil atoms close to the Zr/Ni interface, which in turn is used to determine the values of R_d listed in Table I. It has to be noted that, as it will be discussed in Sec. IV, these values are always greater (even in the case of the irradiation with Ne ions) than those generally used in the literature (10 Å).[20]

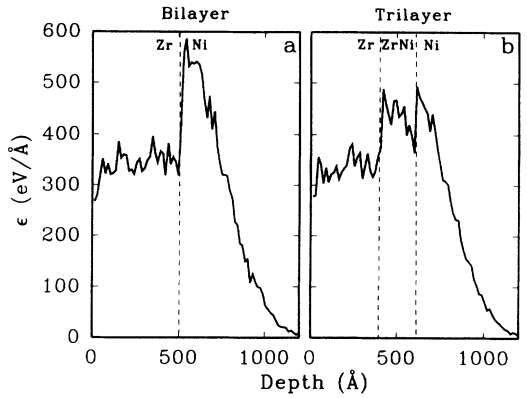

FIG. 1. Depth dependence of the nuclear energy deposition density ε in the case of (a) a Zr/Ni bilayer and (b) a $Zr/Zr_{0.5}Ni_{0.5}/Ni$ trilayer irradiated with 450-keV Xe ions. The calculations have been performed with the TRIM code (Ref. 18).

III. EXPERIMENTAL CONDITIONS

A. Sample preparation

A thin (450–550 Å) layer of Zr was evaporated onto high-purity ⟨100⟩-oriented Ni single crystals in a $\sim 10^{-7}$ Torr vacuum. During evaporation, half of the surface of the crystal was masked in order to keep a Zr-free region for the RBS analysis. Special care was brought to the preparation of the sample to avoid oxidation of the evaporated layer. Specific RBS experiments using the $^{16}O(\alpha,\alpha)^{16}O$ resonant scattering at 3.05 MeV revealed that the concentration of O atoms in the Zr layer was below the detection threshold.

B. Irradiation and RBS analysis

The Zr/Ni samples were mounted on the cold finger of a two-axis liquid-nitrogen-cooled goniometer. They were irradiated at temperatures lower than 100 K with a variety of noble-gas ions of medium energy (see Table I) in the IRMA-CSNSM Orsay implanter. The power density of the ion beam was always kept below 0.5 W/cm^2 to avoid excessive target heating. The temperature of the sample was controlled during irradiation by means of a calibrated Pt resistor. The total irradiation fluence varied from 0.5 to 2×10^{17} atom cm^{-2} depending on the ion used in the experiment.

TABLE I. Irradiation conditions and experimental mixing parameters. ε and R_d are, respectively, the nuclear energy deposition density and the mean projected range of Zr atoms having the average recoil energy, calculated according to the procedure described in Sec. II; $\bar{\nu}_{Zr}$ is the average number of Zr atoms mixed per incident noble-gas ion; $d\sigma^2/d\Phi$ is the mixing rate (see Sec. IV A).

Ion	Energy (keV)	ε (eV/Å)	R_d (Å)	$\bar{\nu}_{Zr}$ (atom/ion)	$d\sigma^2/d\Phi$ (Å^4)
Ne^+	90	54.4	14	0.18	1700
Ar^{2+}	160	100.8	17	0.48	4700
Kr^{2+}	250	265.0	23	1.52	20 800
Xe^{3+}	450	438.0	27	2.46	38 500

The RBS analysis was performed *in situ* at various steps of the irradiation in both random and ⟨100⟩-aligned directions with a 2.4-MeV $^4He^{2+}$ ion beam provided by the ARAMIS-CSNSM Orsay accelerator coupled to the ion implanter.[21] Both parts of the Ni crystals (i.e., covered with Zr and Zr free) were examined. The energy resolution of the experimental setup was ~10 keV, which corresponds to a depth resolution of about 90 Å. The analysis of the random RBS spectra was performed with the RUMP code,[22] whereas the analysis of the aligned spectra was made by using a deconvolution procedure described in Sec. V.

C. Mössbauer experiments

Since channeling does not allow one to determine the nature of the disorder created by ion bombardment, it was essential to investigate the formation of the amorphous layer with a more microscopic technique such as conversion electron Mössbauer spectroscopy (CEMS). This study was achieved on the mixed Zr/Ni samples post-implanted with 20-keV $^{57}Fe^+$ ions (projected range of about 100 Å). Fluences of 4×10^{15} atom cm^{-2} were used in order to record spectra with a reasonable statistics and to keep the final composition of the target almost unchanged. The CEMS measurements were performed at room temperature by using a gas-flow counter with a He-6% CH_4 gas. The Mössbauer source was 25 mCi of ^{57}Co atoms in a Cr matrix. A conventional constant-acceleration Mössbauer spectrometer was used. All isomer shift data are given with respect to the α-Fe standard.

IV. ION-BEAM-MIXING RESULTS

A. Mixing data reduction

The study of the mechanism of ion-beam mixing in the Ni-Zr system does not require the use of the channeling technique and can be made by considering the RBS spectra recorded in a random orientation only (see typical data in Fig. 2). Information concerning the mixing process is generally extracted from the analysis of both the back edge of the Zr profile and the front edge of the Ni signal. In the present work, we have restricted the analysis to the Zr peak, which gives a much better accuracy for the determination of the mixing parameters. Two quantities have thus been extracted: (i) the number of Zr atoms introduced into Ni during irradiation with noble-gas ions (N_{Zr}), determined from the difference in the backscattering yields recorded before and after irradiation beyond the half-width of the back edge of the Zr peak; (ii) the spatial extension of the profile of mixed Zr atoms (σ^2), derived from the least-squares fit of a complementary error function to the Zr peak (solid lines in Fig. 2). The quality of the fits to the random RBS spectra (Zr peak as well as Ni front edge) shown in Fig. 2 demonstrates that such an analysis provides a reasonable description of the mixing process. The variation of N_{Zr} and σ^2 with the irradiation fluence Φ is presented in Fig. 3. The average number of Zr atoms mixed per incident

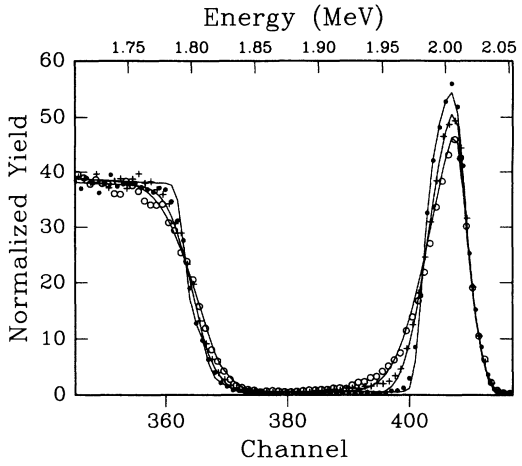

FIG. 2. Random RBS spectra recorded on a Zr/Ni bilayer before (solid circles) and after irradiation at $T<100$ K with 450-keV Xe ions at fluences of 5×10^{15} (crosses) and 10^{16} atom cm^{-2} (open circles). Analyzing particles: 2.4-MeV $^4He^{2+}$ ions. Solid lines are fits to the RBS data by using the RUMP code (Ref. 22).

noble-gas ion ($\bar{\nu}_{Zr}=dN_{Zr}/d\Phi$), as well as the mixing rate ($d\sigma^2/d\Phi$), can be derived from the slopes of the curves of Fig. 3. The values obtained for the various irradiations performed are listed in Table I.

B. Mixing parameters

Figure 4 presents the variation with the nuclear energy deposition density of both the average number of Zr atoms mixed per incident ion, $\bar{\nu}_{Zr}$, and the mixing rate $d\sigma^2/d\Phi$. The two curves exhibit a linear dependence with a threshold value ε_{th} of the order of 20 eV/Å. It should be pointed out that most of the experimental data reported in the literature as well as the predictions of the

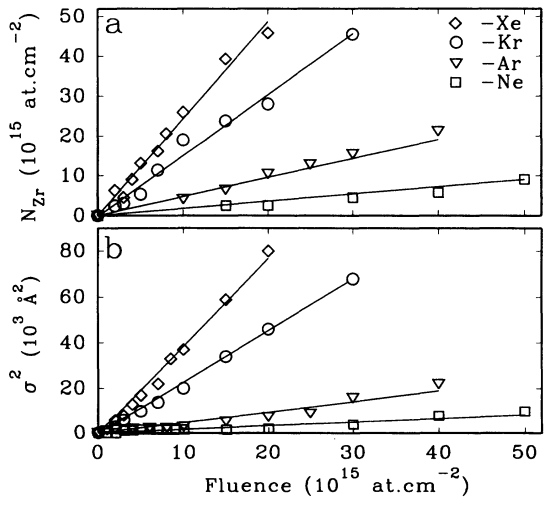

FIG. 3. Ion fluence dependence (a) of the number of Zr atoms mixed into Ni and (b) of the spatial extension of the mixed layer for the various irradiations performed. Solid lines are least-squares fits to the experimental data.

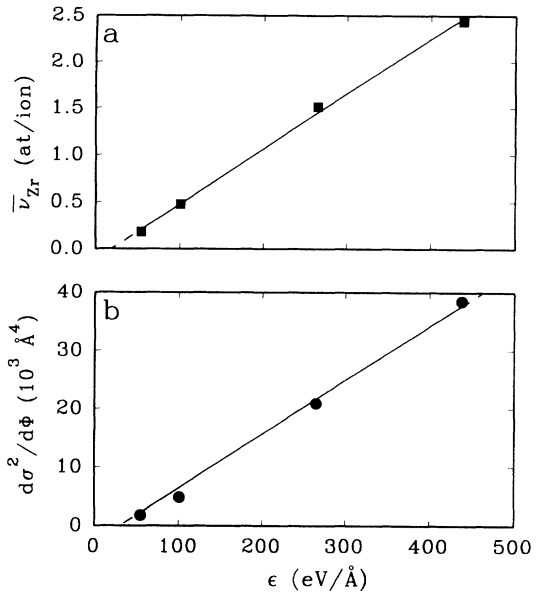

FIG. 4. Variation (a) of the average number of Zr atoms mixed per incident ion and (b) of the mixing rate with the nuclear energy deposition density. Solids lines are least-squares fits to the experimental data.

existing theoretical models (see Sec. IV C) indicate no energy deposition density threshold. However, mixing experiments were generally performed either on bilayered systems irradiated with relatively heavy ions (and consequently high ε values) or on multilayered samples irradiated with light ions (i.e., providing low ε values). In both cases the absence of a threshold value for the mixing process is thus difficult to assess. Moreover, the data obtained in the few experiments which cover a large range of nuclear energy deposition density[23] show that the mixing rates measured for low values of ε are significantly lower than the ones expected if no threshold would exist.

It has to be noted that the same energy deposition density threshold can be found in the curve representing the fluence required for total amorphization of the mixed layer (see Fig. 13 in Sec. V). Since the data related to the disordering of the irradiated sample are recorded almost independently of those concerning the mixing process, this observation provides a strong confirmation of the physical significance of such a threshold. A straightforward (but certainly too naive) interpretation of this result would be that ε_{th} represents a threshold value for the mixing process to occur. In other words, irradiation with very light ions (such that $\varepsilon \leq \varepsilon_{th}$) should not induce any measurable low-temperature mixing of the Zr/Ni bilayer. Another possibility, supported by previous experiments with He ions where small mixing effects were experimentally evidenced,[24] would be to consider at $\bar{\nu}_{Zr}$ and $d\sigma^2/d\Phi$ do not present a sharp threshold, but tend to zero with a lower slope as ε decreases below ε_{th}. Such a decrease of the mixing efficiency at low nuclear energy deposition density should most probably be related to a change in the dominant ion-mixing mechanism.

In the case of a Zr/Ni bilayer, a value of ε of 20 eV/Å corresponds to an irradiation with 50-keV ^{14}N ions (according to the calculations presented in Sec. II). The corresponding average recoil energy of Zr atoms is ~700 eV, leading to a mean projected range of 11 Å. The existence of ε_{th} could then express the fact that Zr atoms displaced at a distance smaller than ~10 Å spontaneously return to their initial position, leading to a negligible mean-square displacement. This interpretation implies that only the atoms displaced at a sufficient distance to avoid athermal recombination with the cascade core vacancies participate to the mixing process. Such a conclusion is consistent with recent molecular-dynamics simulation results,[25] which show that low-energy collision sequences do not induce permanent atomic displacements. A tendency of single interstitial atoms to move back to the cascade core (and consequently to recombine with cascade core vacancies) is observed. Thus the critical step to ensure vacancy-interstitial separation would be the clustering of interstitial atoms on the cascade periphery. Such a mechanism requires a sufficiently high interstitial concentration and, hence, a cascade energy higher than a threshold value. Taking into account the fact that the projected range distribution of recoiling atoms has a Gaussian profile with a standard deviation which can be derived from TRIM simulations, it is possible to calculate the relative fraction of Zr atoms displaced to a distance lower than ~10 Å. At high values of ε, i.e., in the case of heavy-ion irradiation, less than 10% of Zr atoms hit by the incident ions athermally return to their initial position. The relevant parameter to quantify the mixing process is thus R_d, which is proportional to ε [see Eq. (2) of the next subsection]. At ε values lower than ε_{th}, i.e., in the case of light-ion irradiation, an increasing fraction of Zr atoms displaced to a distance less than ~10 Å starts to play a decisive role for the reduction of the measured mixing rate. The mixing process is thus controlled by the number of atoms able to escape from the athermal recombination volume rather than by the value of R_d. If the statistical character of the collisional processes is taken into account, it is clear that, even in the later case concerning very-light-ion irradiation, some atoms will be displaced sufficiently far from their initial site to induce a certain amount of mixing. A direct consequence of the increasing fraction of atoms returning to their initial position is the drastic increase of the irradiation fluence required to obtain a given degree of mixing. Results obtained in experiments using He ions[24] support this assumption.

C. Comparison of the experimental mixing rates to model predictions

The experiments presented in this paper deal with a single system, Ni-Zr, irradiated at low temperature with noble-gas ions of various masses. These considerations lead to the following statements: (i) The nuclear energy density deposited by the irradiating ions ε varies in a rather wide range (from ~50 up to ~450 eV/Å), while the thermodynamical parameters (such as the mixing enthalpy or the effective cohesion energy) remain constant; (ii) the thermally activated transport processes

(such as radiation-enhanced diffusion or radiation-induced segregation) can be ignored. It was thus of particular interest to consider models which discuss the dependence of the mixing parameters with the value of ε. The predictions of the binary collision cascade,[26] cylindrical thermal spike,[27] and nonoverlapping spike[28] models were compared to the experimental results presented above.

In the binary collision cascade model first developed by Sigmund and Gras-Martin,[26] the mixing rate is given by the expression

$$\left[\frac{d\sigma^2}{d\Phi}\right]_{\text{col}} = \frac{1}{3}\Gamma_0 \xi \frac{R_d^2}{\rho E_d}\varepsilon \ , \tag{2}$$

where $\Gamma_0 = 0.608$, $\xi = [4M_1M_2/(M_1+M_2)^2]^{1/2}$, M_1 and M_2 are, respectively, the mass of the incoming ions and the average atomic mass of the target, ρ is the atomic density of the matrix, R_d is the mean range of a displaced atom, and E_d is the average displacement energy. Because of major assumption that collisions can be considered as two-body interactions, the validity of this model is usually considered to be limited to low-density collision cascades. For dense cascades the values of the mixing rates deduced from the binary collision cascade model were generally reported to be an order of magnitude lower than experimental values.[29] However, it has to be pointed out that the relatively low values of the mixing rates obtained in this case are the consequence of the widely accepted assumption that R_d is of the order of 10 Å whatever the ion energy and ion-target combination.[20] As discussed in Sec. II, more accurate calculations of R_d indicate that this value is in general largely underestimated (see Table I). It has also to be noted that, contrary to what is suggested by a rapid survey of Eq. (2), the mixing rate is not a linear function of ε in the case of the binary collision model since the mean projected range of the recoiling atoms is also ε dependent.

In order to take into account the role of thermodynamical effects due to the formation of a new phase by ion-beam mixing, a model based on the assumption that collision cascades overlap to form local liquid zones was developed by Johnson *et al.*[27] The expression of the mixing rate can then be written as

$$\left[\frac{d\sigma^2}{d\Phi}\right]_{\text{ov}} = \frac{1}{2}\left[\frac{k_1}{\rho^{5/3}\Delta H_{\text{coh}}^2}\right]\left[1+\frac{k_2\Delta H_{\text{mix}}}{\Delta H_{\text{coh}}}\right]\varepsilon^2 \ , \tag{3}$$

where ΔH_{coh} and ΔH_{mix} are, respectively, the effective cohesive energy and the mixing enthalpy of the investigated system; k_1 and k_2 are fitting parameters with values of 0.034 Å and 27. It must be noted that in this model the mixing rate is a quadratic function of the nuclear energy deposition density ε.

The assumption of overlapping collision cascades, essential of the model of Johnson *et al.*, is still a matter of controversy. Starting from the same Vineyard expression for the total number of jumps within a spherical spike,[30] Børgesen, Lilienfeld, and Johnson[28] have proposed an expression valid in the case of nonoverlapping spikes. Thus the mixing rate is a linear function of ε:

$$\left[\frac{d\sigma^2}{d\phi}\right]_{\text{lin}} = k_s\psi\left[1+\frac{5}{6}k_2\frac{\Delta H_{\text{mix}}}{\Delta H_{\text{coh}}}\right]\varepsilon \ , \tag{4}$$

where $\psi = Z^{3/2}/\rho^{4/3}\Delta H_{\text{coh}}^{5/3}$ (Z is the average atomic number of the target); k_s is a fitting parameter equal to 0.0347 Å eV$^{2/3}$. The value of k_2 used in this model is generally that of the model of Johnson *et al.* However, a value of 52.4 has also been recently proposed.[31]

The experimental results presented in Sec. IV B suggest to modify Eqs. (2)–(4) in order to account for the energy deposition density threshold found for the mixing process: (i) ε should be replaced by $\varepsilon-\varepsilon_{\text{th}}$; (i) the values of the mixing rate are taken equal to zero for ε values lower than ε_{th}.

Table II compares the values of the mixing rates obtained experimentally to the predictions of the three models considered above. In the case of the binary collision cascade model, the values labeled as "standard" are calculated with a value of R_d equal to 10 Å, while the values labeled as "modified" concern the values of R_d reported in Table I. Figure 5 presents the variation of the mixing efficiency with the nuclear energy deposition density. This figure shows that the best agreement is obtained for the modified binary collision model. Further experiments are now required on other metallic systems to check this correlation.

The mixing efficiencies extracted from the modified binary collision model were compared to the values calculated by Diaz de la Rubia *et al.* using molecular-dynamics simulations.[32] The results obtained for self-irradiated copper are presented in Fig. 6. It is clear that a square-root dependence of the mixing efficiency with the primary recoil energy is obtained in both cases. The

TABLE II. Comparison of the values of the mixing rates determined experimentally and calculated in the framework of the three models mentioned in the text.

	Experimental values	Model predictions for $d\sigma^2/d\Phi$ (Å^4)					
		Binary collision cascade model		Nonoverlapping spike model		Cylindrical spike model	
Ion	$d\sigma^2/d\Phi$ (Å^4)	Standard	Modified	$k_2=27$	$k_2=52.4$	$k_2=27$	$k_2=52.4$
Ne	1700	666	1600	2260	3670	470	790
Ar	4700	1450	4180	4190	6820	1630	2710
Kr	20 800	3980	21 030	10 990	17 890	11 230	18 690
Xe	38 500	6300	42 800	18 160	29 560	30 660	51 030

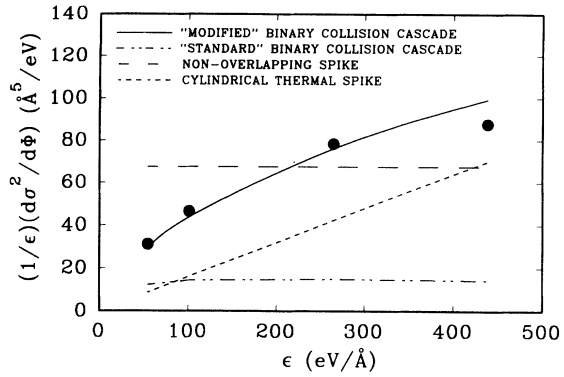

FIG. 5. Variation of the mixing efficiency with the nuclear energy deposition density. Solid circles represent the experimental data; lines indicate the predictions of the theoretical models mentioned in the text.

significantly higher values calculated with the modified binary collision model are in good agreement with the experimental results reported earlier.[14–16]

V. AMORPHIZATION PROCESS

A. Mössbauer results

An experimental confirmation of amorphous phase formation in Ni-Zr irradiated at low temperature with noble-gas ions was provided by CEMS experiments performed on the samples used for the present study. To that purpose, ^{57}Fe atoms were substituted to Ni atoms by room-temperature ion implantation of the Zr/Ni bilayer. Figure 7(a) presents the CEMS spectrum recorded in the case of Kr irradiation. The data were fitted with four quadrupole doublets of respective intensities, quadrupole splittings, and isomer shifts listed in Table III. Doublets D_1 and D_2 are characteristic of the existence of an amorphous Ni-Zr phase of composition varying from a Ni-rich (smaller value of the quadrupole splitting) to a Zr-rich

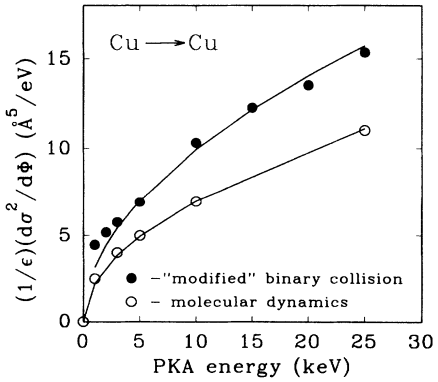

FIG. 6. Variation of the mixing efficiency with the energy transferred to the primary knock-on atom calculated with the "modified" binary collision model (solid circles) or by using a molecular-dynamics simulation (open circles). The molecular-dynamics calculations are taken from Ref. 32.

TABLE III. Characteristics of the quadrupole doublets obtained from the fit to the experimental CEMS spectrum presented in Fig. 7(a).

Doublet	Intensity (%)	Quadrupole splitting (mm/s)	Isomer shift (mm/s)
D_1	43	0.35	−0.05
D_2	31	0.77	0.03
D_3	14	1.47	0.02
D_4	12	1.63	1.17

(larger value of the quadrupole splitting) region. Doublet D_3 is likely related to the strongly perturbed interface region, and doublet D_4 results from partial oxidation of the sample surface.

The CEMS spectra can also be fitted with a distribution of quadrupole splittings P(QS), represented in Fig. 7(b), by using the constrained Hesse-Rubartsch method.[33,34] This distribution exhibits two broad peaks. The larger one, which covers a quadrupole splitting range up to 1 mm/s, is related to the formation of an amorphous phase. The important broadening of the peak suggests a wide composition range for this amorphous phase. The smaller peak, with an average quadrupole splitting of ~1.5 mm/s, can be attributed to the region very close to the Zr/Ni interface.

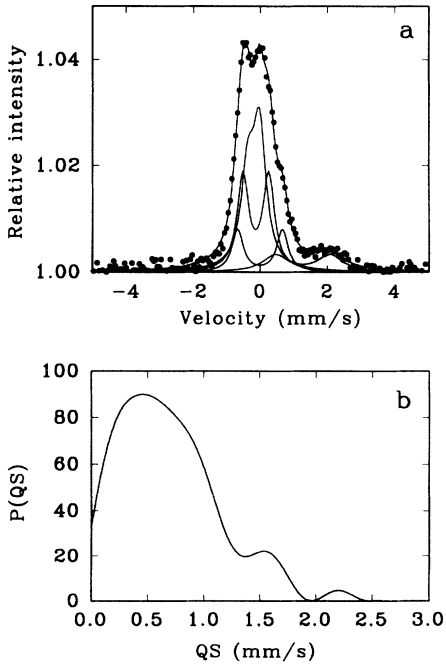

FIG. 7. (a) CEMS spectrum recorded on a Zr/Ni bilayer irradiated at $T < 100$ K with Kr ions at a fluence of 2×10^{16} atom cm^{-2}; the solid line is a fit with the four quadrupole doublets described in the text. (b) Distribution of quadrupole splittings which provides a good fit to experimental data by using the Hesse-Rubartsch method (Refs. 33 and 34).

B. Channeling results

1. Channeling data reduction

Figure 8 presents the Ni signal (the Zr peak is shown in Fig. 2) of typical RBS spectra recorded in random and in ⟨100⟩-aligned orientations on the Zr/Ni sample irradiated with Kr ions. It can be noted that (i) the presence of the deposited Zr layer does not induce a significant degree of dechanneling of the analyzing α particles in the Ni single-crystal substrate before irradiation [the value of the aligned backscattering yield just beyond the surface peak ($\chi_{\min}$) was measured to be, respectively, ~ 0.02 and ~ 0.06 for the Zr-free and Zr-covered parts of the sample]; (ii) noble-gas-ion irradiation leads to the formation of a damage peak in the surface region of the Ni single crystal, with an amplitude increasing with increasing the ion fluence.

The analysis of the damage peak was performed by using a simplified version of the deconvolution procedure described in Ref. 35. The damage depth distribution averaged over the experimental resolution $\bar{d}(x)$ is thus given by

$$\bar{d}(x)=\frac{\chi_a(x)-\chi_d(x)}{\chi_r(x)-\chi_d(x)} , \tag{5}$$

where $\chi_a(x)$ and $\chi_r(x)$ are the backscattering yields at the depth x in the ⟨100⟩-aligned and random spectra, respectively, and $\chi_d(x)$ is the height of the dechanneling fitline which is approximated by the straight line represented in the inset of Fig. 9. The result of this analysis applied to the data obtained for the sample irradiated with Kr ions is presented in Fig. 9 for various irradiation fluences. Quite similar curves are obtained in the case of irradiations with the other noble-gas ions used in the experiment. Since we are mainly interested by the evolution of the damage created in the surface region of the Ni substrate by the mixing of Zr and Ni elements during noble-gas irradiation, the value of $\bar{d}(x)$ close to the Zr/Ni interface (f_d) has been plotted as a function of the irradiation fluence. However, although the depth resolution of the experimental setup is ~ 90 Å, the values

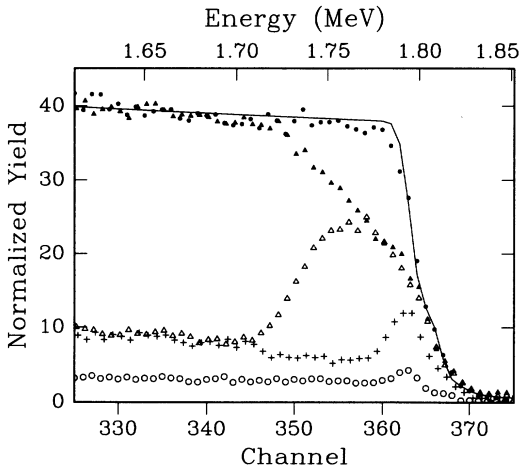

FIG. 8. Ni part of random (solid symbols) and ⟨100⟩-aligned (open symbols and crosses) RBS spectra recorded on a Zr/Ni bilayer irradiated at $T < 100$ K with 250-keV Kr^{2+} ions. Circles, before irradiation; crosses, 10^{16} atom cm^{-2}; triangles, 2×10^{16} atom cm^{-2}. Analyzing particles: 2.4-MeV $^4He^{2+}$ ions. The solid line is a fit to the unirradiated random spectrum by using the RUMP code (Ref. 22).

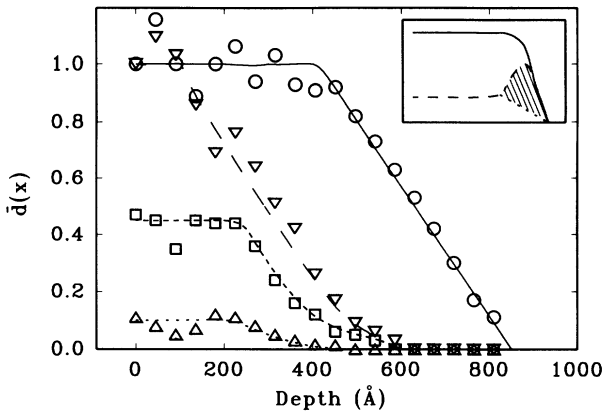

FIG. 9. Depth dependence of the damage distribution $\bar{d}(x)$ [given by Eq. (5) of the text] induced in the Ni single crystal by Kr irradiation. Triangles, before irradiation; squares, 3×10^{15} atom cm^{-2}; inverted triangles, 10^{16} atom cm^{-2}; circles, 5×10^{16} atom cm^{-2}. Lines serve only the purpose to guide the eye. The inset is a schematic representation of the method used to extract $\bar{d}(x)$ from the RBS spectra.

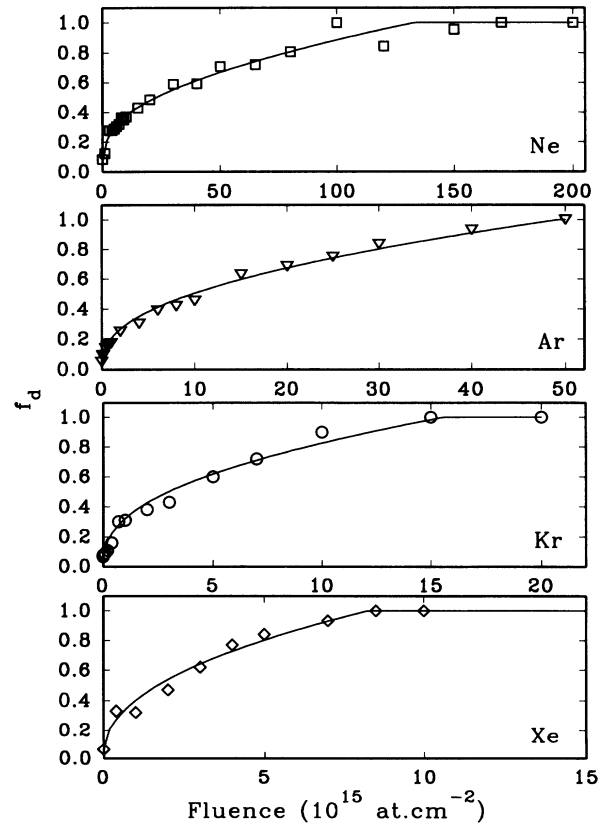

FIG. 10. Ion fluence dependence of the maximum of the damage level in the near-surface region (200 Å thick) of the Ni single crystal for the various irradiations performed. Solid lines represent fits to the experimental data with Eq. (9) of the text.

of f_d were always averaged over a thickness of 200 Å in order to minimize the uncertainties due to the statistical character of the RBS technique. Figure 10 presents the result of such a plot for the different irradiations performed. It is worth noting that in all cases a rather sharp increase of f_d is observed at low irradiation fluences, followed by a slower increase up to unity. Further increase of the irradiation fluence does not affect the value of f_d.

2. *Analysis of the dechanneling yields*

Before discussing the method used to analyze the dechanneling yields presented in Fig. 10, it is important to emphasize some of the experimental limitations: (i) The real depth sensitivity of channeling experiments is ~200 Å (see RBS data reduction in Sec. V B 1); (ii) channeling alone does not allow one to determine the nature of the disorder created by the irradiation. Nevertheless, the knowledge of the irradiation properties of metallic alloys provides indications concerning the disordering behavior of the Ni-Zr system. The sharp initial increase of the dechanneling yields (for ion fluences ranging from 0 up to $\sim 10^{15}$ atom cm^{-2} in the case of Kr irradiation), which saturates at a relatively low level (~ 0.15), is typical of the dechanneling occurring in irradiated pure metals and has already been observed in self-irradiated Ni single crystals.[3] In the intermediate fluence range (10^{15}–1.5×10^{16} atom cm^{-2} in the case of Kr irradiation) where the channeling yields increase nearly linearly with the irradiation fluence, the consideration of previous results obtained on irradiated Zr/Ni bilayers[14–16] as well as the CEMS data presented in Sec. V A lead to the conclusion that an amorphous Ni-Zr phase is progressively formed in the mixed layer. However, it must be noted that, as a result of the depth sensitivity of the RBS technique, it is impossible to distinguish whether a whole 200-Å-thick layer is partially amorphized or a thinner totally amorphous layer is formed at the interface and grows inside the Ni substrate as the irradiation fluence increases. In both cases the results obtained by using the channeling technique would be the same: a value of f_d lower than unity. As a consequence, in the following discussion the term "amorphous fraction" should always be understood as the fraction of amorphous phase in a 200-Å-thick Ni layer close to the Zr/Ni interface.

The quantitative analysis of the disordering process in ion-beam-mixed Ni-Zr requires an hypothesis concerning the structure of the mixed layer. From the considerations developed above, it is assumed that this layer is composed of amorphous (fraction A_m) and (virgin or partly disordered) crystalline [fraction $(1-A_m)$] regions. Thus the scattering of analyzing α particles in the surface layer of the Ni single crystal arises from three major contributions: (i) the scattering on the first atomic layers in the crystalline part of the sample (leading to the so-called surface peak), (ii) the scattering due to radiation defects produced in the crystalline part of the surface layer by the incoming ions, and (iii) the scattering on the amorphous zones formed during mixing.

The scattering contribution due to the first atomic layers of the crystal ($f_{\rm SP}$) is simply the product of the value of f_d measured on an unirradiated crystal ($f_{\rm unirr}$) and of the crystalline fraction of the sample:

$$f_{\rm SP}=f_{\rm unirr}(1-A_m)\ . \tag{6}$$

Since the value of $f_{\rm unirr}$ is typically 0.06, the correction brought by the surface peak contribution to the total scattering is always very small.

The production of radiation damage in metals by ion irradiation has been extensively studied in the past years, mainly by electrical resistance experiments. The production rate was shown to increase almost linearly at low fluence with an exponential saturation at a relatively low level (compared to the case of semiconductors or insulators). This behavior is due to both the large athermal recombination volume of point defects in metals and the high mobility of self-interstitial atoms (even at 100 K). In the present experiment, the contribution due to the scattering on radiation defects created in the crystalline phase ($f_{\rm def}$) was evaluated by considering the result obtained on the Zr-free part of the sample (see Fig. 11):

$$f_{\rm def}=d_s[1-\exp(-\sigma_d\Phi)](1-A_m)\ , \tag{7}$$

where d_s is the saturation value for the scattering on radiation defects, Φ is the irradiation fluence, and σ_d is the cross section for radiation defect creation. It must be pointed out that the presence of Zr atoms may influence the saturation concentration of defects in the crystalline Ni matrix. Thus, as will be discussed later on, the parameters d_s and σ_d were kept free to vary during the fitting procedure.

The amorphous zones formed in the surface layer of the Ni crystal during ion mixing give rise to a direct scattering of the channeled fraction of analyzing α particles.[35] The backscattering factor is equal to 1, so that the scattering contribution due to the amorphous part of the crystal can be written

$$f_{\rm am}=A_m\ . \tag{8}$$

It has been shown in Sec. IV that the profile of Zr atoms introduced into the Ni crystal by ion-beam mixing can be described by using a complementary error function. The assumption that the crystalline-to-amorphous

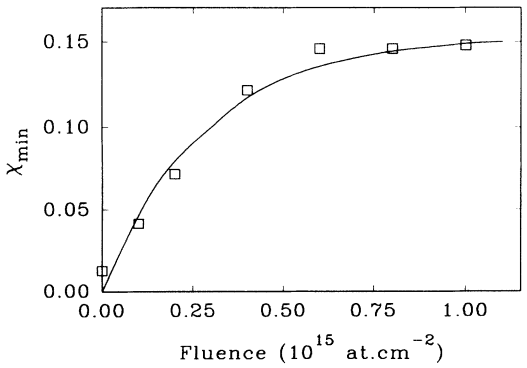

FIG. 11. Ion fluence dependence of the aligned backscattering yield recorded just behind the surface peak for a pure Ni single crystal irradiated at $T < 100$ K with 160-keV Ar ions.

phase transformation occurs as the Zr concentration corresponds to the glass-forming range for the Ni-Zr system[15] allows one to calculate the thickness of the amorphous layer formed by mixing (x_{am}) from the values of σ^2. The result of such a calculation is presented in Fig. 12 as a function of the number of mixed Zr atoms (N_{Zr}). One can note a square-root variation of the amorphous phase thickness versus N_{Zr}, which is a result of the linear dependence of σ^2 with the irradiation fluence [see Fig. 3(b)]. The fact that the data relative to the different irradiations fit a unique curve in Fig. 12 provides the demonstration that the number of mixed atoms monitors the formation of the amorphous phase.

The establishment of a relationship between the spatial development of the amorphous layer formed through ion mixing and the irradiating ion fluence comes up against a severe boundary condition problem. The description of the mixing profile by the use of a complementary error function suggests a low fluence continuity in the formation of the amorphous layer. However, this hypothesis is physically unacceptable. A discontinuity must exist, since an amorphous layer cannot be defined over a thickness lower than, e.g., a few interatomic distances. The existence of a thickness threshold for the formation of the amorphous layer implies the existence of a fluence threshold for amorphization (Φ_c). The assumption that the thickness threshold is the correlation length of an amorphous material, of the order of 10 Å, leads to a value of $\Phi_c \sim 1.2\times10^{15}$ atom cm^{-2} in the case of Kr irradiation. Thus, at very low irradiation fluences, i.e., at fluences such that the thickness of the amorphous layer calculated with an erfc distribution would be lower than 10 Å, amorphous phase formation does not occur. At ion fluences above Φ_c but below the fluence required to mix a layer of thickness corresponding to the depth sensitivity of RBS experiments $x_0=200$ Å, the real thickness of the amorphous layer formed cannot be deduced from the analysis of the RBS spectra and its contribution to the dechanneling yield is proportional to x_{am}/x_0. At higher irradiation fluences, i.e., at fluences such that x_{am} exceeds 200 Å, the thickness of the amorphous layer can be derived directly from the RBS data and its contribution to the scattering yield is equal to 1.

Equations (6)–(8) and the considerations developed above lead to the following expression for the total scattering occurring in the surface layer of the irradiated Zr/Ni samples:

$$f_d = A_m + (1-A_m)\{f_{\text{unirr}} + d_s[1-\exp(-\sigma_d\Phi)]\} , \quad (9)$$

where

$$A_m = \begin{cases} \xi_{am}[\nu_{Zr}(\Phi-\Phi_c)]^{1/2}/x_0 & \text{for } x_{am} < x_0 , \\ 1 & \text{for } x_{am} \geq x_0 . \end{cases} \quad (10)$$

In Eq. (10), ξ_{am} is a parameter which quantifies the growth rate of the amorphous layer formed by ion-beam mixing for the system considered in the present experiment.

Equation (9) contains three parameters d_s, σ_d, and ξ_{am}. A value of ξ_{am} could be *a priori* calculated from the values of the glass-forming range of the Ni-Zr system found in the literature and the mixing rates reported in Sec. IV. However, we have chosen to keep this parameter free to vary during the fitting procedure in order to avoid the ambiguities arising from the choice of the values of the glass-forming range. The results of the fits to the experimental data are represented by the solid lines appearing in Fig. 10. The best fits were obtained for $\xi_{am}=54.2$ Å/$[(10^{15}$ atom cm$^{-2})]^{1/2}$. It is worth noting that the limits of the glass-forming concentration of the Ni-Zr system calculated with the values of ξ_{am} obtained from the fits are 0.10 and 0.90, in perfect agreement with the existing data.[15]

An interesting quantity which can be derived from the data reported in this paper is the critical ion fluence (D_{am}) required to amorphize a given thickness of the Ni substrate (arbitrarily chosen here as the depth sensitivity of the RBS technique $x_0=200$ Å) by ion-beam mixing. The variation of D_{am} with the nuclear energy deposition density is presented in Fig. 13. The behavior versus ε of

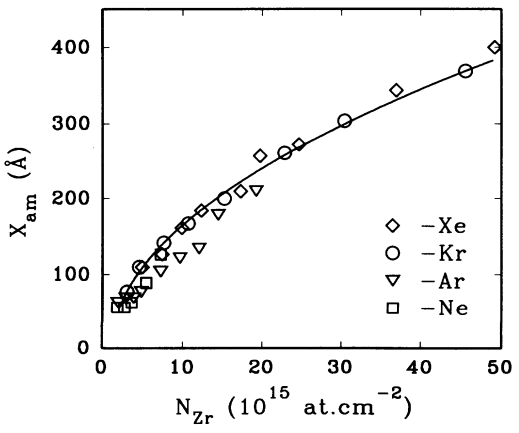

FIG. 12. Thickness of the amorphous layer formed during the mixing process vs the number of Zr atoms mixed by noble-gas-ion irradiation.

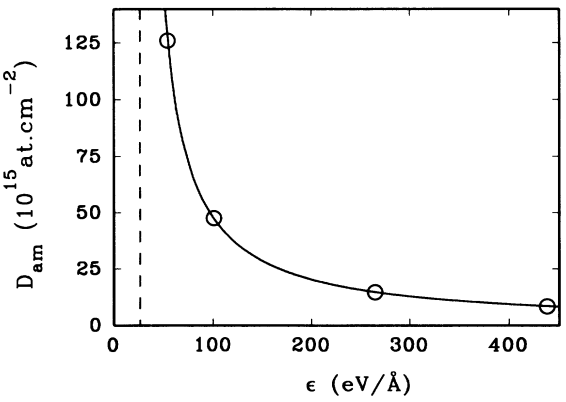

FIG. 13. Critical ion fluence for amorphization of a layer of thickness $x_0=200$ Å as a function of the nuclear energy deposition density for the various irradiations performed. The solid line is a fit to the data with the function indicated in the text. The dashed line represents the threshold value of ε for the formation of an amorphous phase.

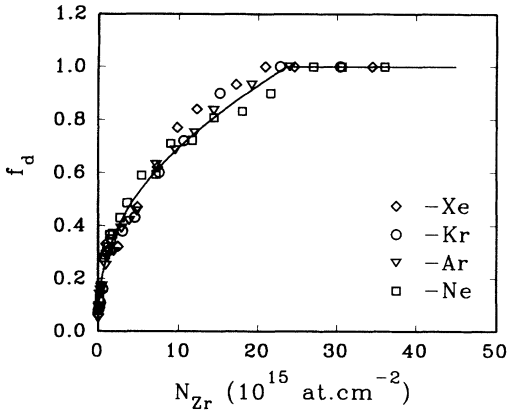

FIG. 14. Damage level in the near-surface region (200 Å thick) of the Ni single crystal vs the number of Zr atoms mixed by the various noble-gas ions used for the irradiations. The solid line is a fit to the experimental data by considering the three dechanneling contributions mentioned in the text.

the critical fluence for amorphization confirms the mixing results reported in Sec. IV. The solid line in Fig. 13 represents the fit to the data with a function $f(\varepsilon)=a/(\varepsilon-b)$. The choice of this fitting function is justified by the linear increase of the number of mixed Zr atoms versus ε [Fig. 4(a)]. A threshold value of $\varepsilon \sim 20$ eV/Å is obtained (dashed line in Fig. 13), indicating that the amorphization process requires a minimum energy transfer to the primary knock-on atoms. This observation supports the hypothesis of the existence of a nuclear energy density threshold for the low-temperature mixing process, discussed in Sec. IV.

C. Amorphization mechanisms by ion-beam mixing

Since the rates of increase with the noble-gas fluence of (i) the scattering occurring in the surface region of the Ni crystal as amorphization sets in (Fig. 10) and (ii) the parameters which quantify the mixing process (Fig. 3) seem to be strongly correlated, it was interesting to plot f_d as a function of N_{Zr} for the various irradiations performed. The result is presented in Fig. 14. This figure provides a striking evidence that the number of mixed atoms is the parameter which governs the amorphization process. Such a behavior can be explained by the formation of a Ni-Zr alloy in which the damage level is related to the concentration of Zr atoms introduced into Ni by mixing (similarly to the case of direct implantation experiments), rather than to the number of atomic displacements induced by elastic collisions (as in the case of irradiation experiments).[8,9] Once the amorphous phase has been formed, further irradiation leads to an increase of the thickness of the amorphous layer, as demonstrated in Fig. 9. This conclusion is corroborated by the linear increase of σ^2 with the ion fluence exhibited in Fig. 3(b).

The results described in this paper allow one to propose a possible mechanism for the amorphization process by ion-beam mixing. Before irradiation, the original configuration consists of a Zr layer deposited on a Ni substrate with a sharp interface [Fig. 15(a)]. In the early stages of the irradiation, both Zr and Ni atoms move in opposite directions to form a mixed layer with a disordered crystalline structure [Fig. 15(b)]. It is very likely that the thickness of this layer corresponds to the projected range of Zr or Ni atoms having a recoil energy close to the average value. As it was calculated in Sec. II, this range varies from 14 Å for 90-keV Ne irradiation to 27 Å in the case of 450-keV Xe irradiation. As irradiation progresses, both the number of mixed atoms and the spatial extension of the mixed layer increase. Thus, as the concentration of both components in the region near the Zr/Ni interface reaches the concentration range for glass formation, a crystalline-to-amorphous transformation occurs. By analogy with the case of direct ion-implantation experiments,[8,9] it can be considered that a partially amorphous structure (with the presence of small amorphous clusters) is formed in a first step [Fig. 15(c)]. Then total amorphization of this layer occurs by the coalescence of the amorphous clusters formed [Fig. 15(d)]. Here it must be once more emphasized that, as a result of the depth sensitivity of the RBS experiments, the formation of an amorphous layer with a thickness x_{am} lower than ~ 200 Å does not correspond to a value of $f_d=1$ in the curves of Fig. 10. A further increase of the irradiation fluence then leads to an increase of the thickness of the amorphous layer formed by mixing [Fig. 15(e)]. As x_{am} reaches 200 Å, the level of the disorder peak present in the aligned RBS spectra fits the random level ($f_d=1$ in the surface region of the Ni signal), and

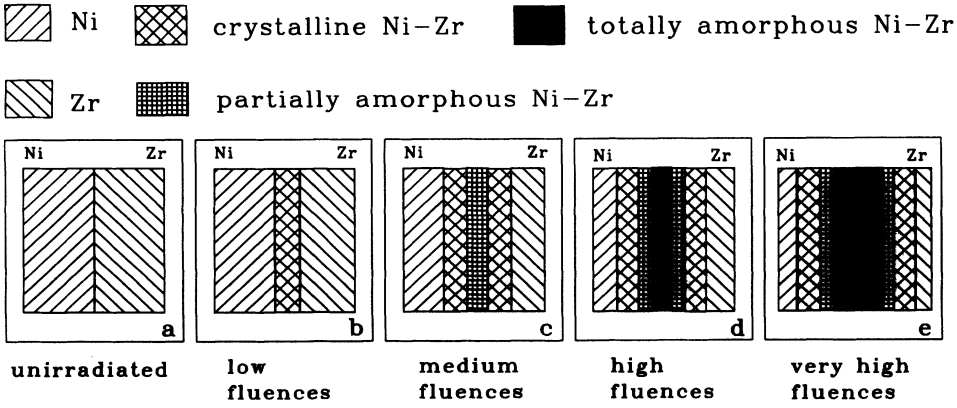

FIG. 15. Schematic representation of the spatial evolution of a Zr/Ni bilayer submitted to irradiation with noble-gas ions at low temperature.

further changes of the amorphous layer thickness become measurable experimentally. Of course, the bottom and top of the Zr and Ni distributions constitute regions of composition out of the glass-forming range and remain crystalline [cross hatched areas in Figs. 15(c)–15(e)].

VI. CONCLUSION

The RBS and channeling experiments presented in this paper have allowed us to propose a description of the amorphization processes occurring during ion-beam mixing of a crystalline metallic bilayer.

The mixing results show very interesting features, such as a nuclear energy deposition density threshold of 20 eV/Å probably due to a change in the mixing mechanism for very-light-ion irradiation. The comparison between the mixing efficiencies determined experimentally and the model predictions indicates that the description in terms of binary collision cascades with values of the parameters ε and R_d determined from Monte Carlo simulations gives the best accuracy in the case of low-temperature irradiation. A good agreement can also be noted between the results obtained by using a "modified" binary collision model and molecular-dynamics computer simulations. The consistency of our experimental data with the interpretation proposed by English *et al.*[25] indicates the importance of the collisional phase of displacement cascades for the mixing mechanism. The main advantage of the calculations presented in this paper is that the algorithm used is much simpler and does not require time-consuming calculations on mainframe computers as is the case for molecular-dynamics simulations.

Concerning the amorphization process, it is clear that the concentration of foreign atoms introduced by mixing controls the amorphization kinetics, i.e., the variation of the amorphous fraction with the irradiation fluence. The damage created during the mixing process contributes only to maintain the bombarded lattice in constant atomic agitation. This behavior is comparable to the case of direct ion implantation where function g of Eq. (1) was demonstrated to monitor amorphization (contrary to the case of ion irradiation where the function f has been proven to be operative). However, the present results show that the spatial extension of the amorphous layer is quite different in both types of experiments. In ion implantation, amorphization starts around the ion-projected range and extends toward both the sample surface and greater depth as implantation progresses. On the contrary, ion-beam mixing leads to the formation of an amorphous layer at the interface between the two elements and develops in depth as the irradiation fluence increases (Fig. 15). The thickness of the amorphous layer formed in this case is a square-root function of the number of mixed atoms. Thus the kinetics of amorphous phase formation can be accounted for by an equation taking into account the number of mixed atoms per incident ion and the concentrations of the glass-forming range for the system considered. Obviously, a threshold thickness for the formation of an amorphous layer exists. Our experiments do not allow us to provide a measurement of this threshold thickness, which has been approximated to ~ 10 Å.

The last question concerns the influence of the bombardment temperature on the processes leading to amorphous phase formation by ion-beam mixing. The experiments reported here were performed below 100 K, i.e., in a temperature range where radiation-enhanced diffusion of one of the two species is avoided. It is very likely that at higher temperature the composition of the phase thermodynamically favored plays a decisive role in the spatial development (or the absence) of the amorphous phase. Similar experiments, where the temperature of the sample is varied during irradiation, are in progress to elucidate this point.

ACKNOWLEDGMENTS

We want to thank Professor Gras-Marti for interesting comments concerning the interpretation of mixing results, Professor Kopcewicz for CEMS analysis, and B. Vassent for sample preparation. We are grateful to the SEMIRAMIS group of the CSNSM-Orsay for their assistance during the experiments and to H. Bernas for his precious help for obtaining beam time at the ARAMIS accelerator.

[1]The most recent review paper concerning amorphous phase formation in particle-bombarded metallic systems is P. M. Ossi, Riv. Nuovo Cimento **15**, 1 (1992).
[2]V. Heera and B. Rauschenbach, Radiat. Eff. **91**, 71 (1985).
[3]C. Cohen, A. Benyagoub, H. Bernas, J. Chaumont, L. Thomé, M. Berti, and A. V. Drigo, Phys. Rev. B **31**, 5 (1985).
[4]E. P. Simonen, Nucl. Instrum. Methods B **16**, 198 (1986).
[5]G. Linker, Nucl. Instrum. Methods B **19/20**, 526 (1987).
[6]D. F. Pedraza, Mater. Sci. Eng. **90**, 69 (1987).
[7]H. Hsieh and S. Yip, Phys. Rev. B **39**, 7476 (1989).
[8]For a review, see L. Thomé, in *Nuclear Physics Applications on Materials Science,* Vol. 144 of *NATO Advanced Study Institute, Series E: Applied Sciences,* edited by E. Recknagel and J. C. Soares (Kluwer, Dordrecht, 1988), p. 183.
[9]A. Benyagoub and L. Thomé, Phys. Rev. B **38**, 10 205 (1988).
[10]S. Matteson and M. A. Nicolet, Annu. Rev. Mater. Sci. **13**, 339 (1983).
[11]B. M. Paine and R. S. Averback, Nucl. Instrum. Methods B **7/8**, 666 (1985).
[12]B. X. Liu, Phys. Status Solidi A **94**, 11 (1986).
[13]S. J. Kim, M. A. Nicolet, R. S. Averback, and D. Peak, Phys. Rev. B **37**, 38 (1988).
[14]F. R. Ding, P. R. Okamoto, and L. E. Rehn, J. Mater. Res. **4**, 1444 (1989).
[15]J. Bøttiger, K. Dyrbye, K. Pampus, and R. Poulcen, Philos. Mag. A **59**, 569 (1989).
[16]R. de Reus, A. M. Vredenberg, A. C. Voorrips, H. C. Tissink, and F. W. Saris, Nucl. Instrum. Methods B **53**, 24 (1991).
[17]L. Thomé, T. Benkoulal, J. Jagielski, and B. Vassent, Europhys. Lett. **20**, 413 (1992).
[18]J. P. Biersack and L. G. Haggmark, Nucl. Instrum. Methods **174**, 257 (1980).

[19]The justification of the choice of the thickness over which calculations are performed is provided in Sec. V.
[20]H. H. Andersen, Appl. Phys. **18**, 131 (1979).
[21]E. Cottereau, J. Camplan, J. Chaumont, R. Meunier, and H. Bernas, Nucl. Instrum. Methods B **45**, 293 (1990).
[22]L. R. Doolittle, Nucl. Instrum. Methods B **9**, 5008 (1985).
[23]F. Shi, T. Weber, W. Bolse, and K-P. Lieb, Appl. Phys. A **57**, 343 (1993).
[24]M. G. Le Boité, A. Traverse, L. Névot, B. Pardo, and J. Corno, J. Mater. Res. **3**, 1089 (1988).
[25]C. A. English, A. J. E. Foreman, W. J. Phytian, D. J. Bacon, and M. L. Jenkins, Mater. Sci. Forum **97-99**, 1 (1992).
[26]P. Sigmund and A. Gras-Marti, Nucl. Instrum. Methods **168**, 389 (1980); **182/183**, 25 (1981).
[27]W. L. Johnson, Y. T. Cheng, M. Van Rossum, and M. A. Nicolet, Nucl. Instrum. Methods B **7/8**, 657 (1985).
[28]P. Børgesen, D. A. Lilienfeld, and H. H. Johnson, Appl. Phys. Lett. **57**, 1407 (1990).
[29]I. Koponen and M. Hautala, Nucl. Instrum. Methods B **69**, 182 (1992).
[30]G. H. Vineyard, Radiat. Eff. **29**, 245 (1976).
[31]P. Børgesen, D. A. Lilienfeld, and H. Msaad, Nucl. Instrum. Methods B **59/60**, 563 (1991).
[32]T. Diaz de la Rubia, R. S. Averback, H. Hsieh, and R. Benedek, J. Mater. Res. **4**, 579 (1989).
[33]J. Hesse and A. Rubartsch, J. Phys. E **7**, 526 (1974).
[34]G. Le Caer and J. M. Dubois, J. Phys. E **12**, 1083 (1979).
[35]L. C. Feldman, J. W. Mayer, and S. T. Picraux, *Materials Analysis by Ion Channeling* (Academic, New York, 1982).

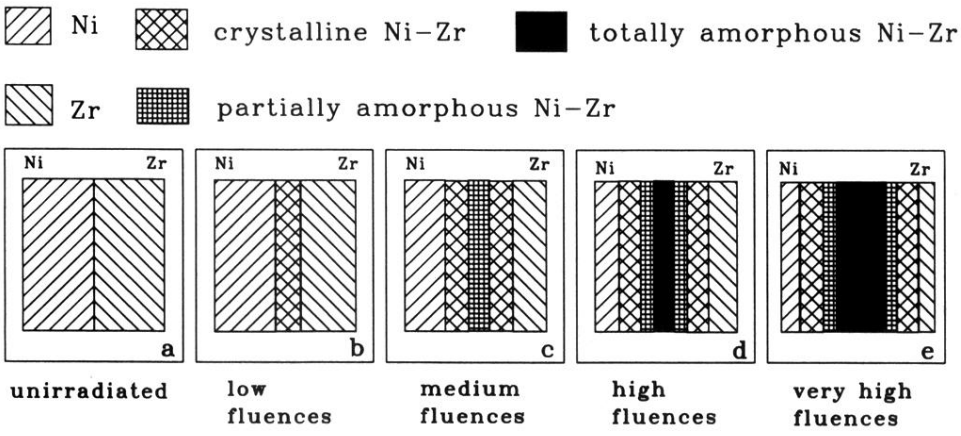

FIG. 15. Schematic representation of the spatial evolution of a Zr/Ni bilayer submitted to irradiation with noble-gas ions at low temperature.